

Modeling and Identification of Load-Dependent Properties for Electrically Preloaded Rack-and-Pinion Drives

Valentin Leipe¹, Lukas Steinle¹, Xabier Agirre Bikuña^{1,2}, Armin Lechler¹, and Alexander Verl¹, *Member, IEEE*

Abstract—Rack-and-pinion drives are preferred feed drives for long travel distances and heavy loads in large machine tools. One of the advantages compared to other feed drive systems is consistent stiffness regardless of travel length. A primary challenge with rack-and-pinion drives is the achievable accuracy due to backlash. To compensate for backlash, electrically preloaded systems are commonly used in machine tools. In the case of electrical preload between two motors, the system is more complex to identify because the feed drive specific properties cannot be directly assigned to the respective drive train. To address this issue, this paper presents a novel method for modeling and identifying the load-dependent stiffness and damping of an electrically preloaded system. For this purpose, a mathematical modeling based on experimental data from a test bench with industrial components is presented to separate the drive train specific properties. This allows the system behavior to be modeled more accurately and used for control approaches.

I. INTRODUCTION

In machine tools, feed drives are a key component in performing manufacturing tasks. Various types of drive systems are available to generate the movement of the machine tool. The motion of the feed drive is mainly generated by electromechanical servo drive systems. Motors with a transmission element are used to convert the rotational motion of the motor into translational motion. A ball screw drive (BSD) or rack-and-pinion drive (RPD) is commonly used as the mechanical transmission element for feed drive systems [1]. The appropriate drive system is selected according to the application. The BSD is characterized by high efficiency, but the stiffness is position dependent [2]. This leads to locally varying dynamics of the system [3] and is therefore a challenge for model-based control.

RPDs are usually used when a feed drive for long travel distances is required [4]. The stiffness and inertia of these feed drives are independent of the travel distance [1]. RPDs are therefore widely used for large scale manufacturing processes where long travel distances and high load requirements need to be managed.

One of the biggest challenges with RPDs is backlash, as it affects their overall dynamic properties [5] and reduces

accuracy. Backlash occurs when the direction of motion between the rack and pinion is reversed. This causes the tooth flank of the pinion to change the tooth flank side of the rack and the motor momentarily stops transmitting force to the machine table. As a result, there is no contact between the rack and the pinion and the machine table is in a non-controllable state. The backlash affects the achievable accuracy of the drive system as well as the control quality due to the nonlinear transmission behavior [6].

To compensate backlash, various mechanical and electrical preload techniques have been suggested in the literature. Mechanical preload can be realized with a split pinion on the drive shaft, with both pinions in contact with the opposite flank of the rack [3] or with two pinions and a respective gearbox, where the gearboxes are connected by a flexible coupling [7]. Mechanical preload is a passive preload and cannot be changed during operation. In addition to mechanical preload, there is also electrical preload, which is mainly used in industry and is also used in this paper. Electrical preload requires two motors, each with a pinion, which are preloaded against each other in opposite directions with an additional torque. In the industry, a constant preload torque is chosen for the electrical preload. It is typically in the range of 10% to 30% of the rated motor torque [8]. However, it is beneficial to vary the preload during operation to maximize the dynamics of the drive system [1]. This property was presented in [6] and a novel adaptive preload control to increase energy efficiency for RPDs was shown.

Compared to the BSD, the RPD has no position-dependent stiffness. Any number of racks can be lined up to realize a travel distance of any length [9]. However, the stiffness between the rack and pinion depends on the load [10]. The components and in particular the tooth flanks deform due to additional forces [11]. Under operating conditions with high process forces or heavy workpieces, some of the loads may be high and cause tooth deflection and thus deformation of the contact line, resulting in varying stiffness [12]. The load changes the contact surface between the rack and pinion, which affects the stiffness and therefore the system dynamics, as the stiffness has a central influence on the motion quality and transmission behavior of the drive system [1]. For each single tooth, the contact force moves along a line due to the involute shape and the contact stiffness takes a nonlinear shape along this contact line [13]. As the load increases, the contact width and therefore the stiffness of the system changes [13].

This work was funded by the Deutsche Forschungsgemeinschaft (DFG, German Research Foundation), Project No. 462185026 and 286294048. The authors gratefully acknowledge the support by DFG.

¹ The authors are with the Institute for Control Engineering of Machine Tools and Manufacturing Units, University of Stuttgart, Stuttgart 70174, Germany, valentin.leipe@isw.uni-stuttgart.de

² Mondragon Unibertsitatea - Faculty of Engineering, Loramendi 4, 20500, Arrasate-Mondragon, Spain

As well as the stiffness, the damping of the whole system also varies with the contact area. Neglecting the backlash, the following three-mass oscillator shown in Fig. 1 can be assumed for a preloaded system. We follow the convention that the motor variables are denoted with index $(\cdot)_1$ for motor 1, $(\cdot)_2$ for motor 2, the table variables with $(\cdot)_T$ and friction with $(\cdot)_F$. The stiffness k and damping d are shown in the figure as load-dependent and therefore vary depending on the motor torque. The motor torque τ_i can be converted via the gearbox ratio i_g and the pitch diameter d_p into a force with $F_i = 2 \cdot i_g / d_p \cdot \tau_i$.

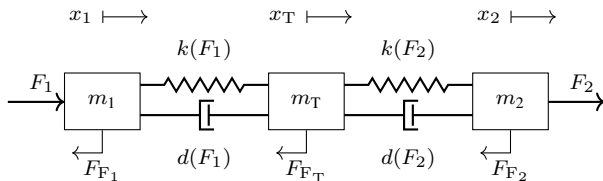


Fig. 1. Schematic model of the electrically preloaded rack-and-pinion drive.

When identifying the stiffness and damping on a physical machine with industrial hardware, the two springs and dampers are considered in combination. However, this represents the total stiffness and damping of the whole system, whereas distributing the stiffness and damping between the two drive trains remains a challenge. There is no approach in the literature that describes how the determined total contribution is distributed between the two individual drives. This is investigated in this paper. The novelty is the general approach to determine the load-dependent stiffness and damping of each drive train for preloaded rack-and-pinion drives, and thus the distribution of the overall properties to the individual ones.

II. CONTROL OF PRELOADED SYSTEMS

The control structure of a preloaded system used in this paper is described in the following. The machine table is controlled by an industry-standard cascade controller. This controller consists of three nested control loops [8]. The inner control loop must always be faster than the outer one. From the inside control loop to the outer, the cascade controller consists of a current controller, a velocity controller and a position controller. In a preloaded system, the control structure is extended to include another cascade controller for the second drive train (see Fig. 2), but the desired velocity v_d is provided by a common position controller [14]. A velocity preload controller is used to electrically preload the two drives against each other. The preload controller, which is a P controller, generates a preload torque by applying an additional velocity v_p to the corresponding PI velocity controller of each drive train. For one drive train the additional velocity is added and for the other subtracted to achieve the preload. The velocity controller then controls the velocity error between the desired velocity v_d and the actual motor velocity v_i . The preload torque is calculated by considering half of the desired torques τ_{d_i} of the velocity

controllers (due to identical motors) and a constant preload torque value τ_p , which determines the preload between the two drive trains. τ_p can be used to set various preloads in the system, which are later required for system identification. The velocity preload controller leads to a constant preload between the two drive trains and thus to a change in motor force. The torque is then controlled by a PI current controller and the motors are actuated. In Fig. 2 the controlled system with the preload controller is shown.

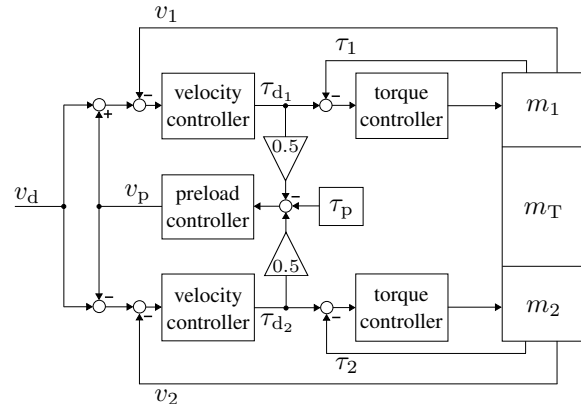


Fig. 2. Block diagram of the preload control structure based on [6].

III. SYSTEM IDENTIFICATION

To increase the dynamic accuracy of machine tools, it is important to analyze the dynamic properties of the system used. With the help of the analysis, the dynamic behavior can be identified and thus modeled. Especially in the case of electrically preloaded RPDs, a more detailed investigation of the impact of both drives is required due to the preload in order to determine the preload-dependent properties.

In [5] the dependence of the stiffness on the driving force was investigated. For this purpose, the machine table was positioned against a mechanical stop and an increasing drive force was applied to the torque-controlled motor. This deforms the respective drive and statically determines the stiffness using the measurement signals from the motor and the table. In the state of the art it is shown that the preload has an effect on the stiffness, which can be calculated and represented using Hooke's law $k = F/\Delta x$. In [15] a method for determining the mesh stiffness in cylindrical tooth pairs is presented. It is shown that the stiffness is nonlinear with an increase in force due to the contact area [15]. Contact stiffness can also be simulated using FE models and has been shown in [16]. This allows an initial estimate of the stiffness curve as a function of force to be analyzed and shows a nonlinear shape. The nonlinear behavior of mesh stiffness, considering contact deflections, is approximated by an analytical function in [17]. An ansatz function of the stiffness curve is also determined and identified in the presented paper.

In contrast to load-dependent stiffness, there is less information available in the literature on load-dependent damping.

In [18] a decreasing damping for higher velocities is shown. From this, it can be deduced that the damping will also exhibit a nonlinear behavior and a hyperbolic shape is assumed in this paper.

In [5], the dynamic properties of the rack-and-pinion drive were investigated under the influence of various preloads. The varying system behavior during preload changes was demonstrated and is now being used to identify the load-dependent stiffness and damping of the system as a function of contact force for use in modeling new approaches. The function is defined for each drive train and the total contribution determined must be distributed to the corresponding one. The dynamic stiffness as well as the damping are identified in the frequency domain. For this purpose, the natural frequency of the amplitude response is used for different preloads. The mechanical transfer function is used to determine the stiffness and damping from the frequency response. This transfer function is defined so that the input is the velocity of one motor, in our case the velocity of motor 1 v_1 , and the output is the table velocity v_T . The frequency transfer function (FTF) of the compliant mechanics is defined in the Laplace domain as $G(s) = V_T(s)/V_1(s)$ using a spectral density estimate of H_3 [19] with a Hamming window of length 1024 and window overlap of 717 samples. To obtain the frequency response, a sine sweep is applied to the target velocity. This signal excites different frequencies. The measurement is then repeated for different preload torques. Whereby a percentage value of the rated motor torque is set. In this way, the load-dependent stiffness and damping can be identified so that they can be modeled by approximating a mathematical function.

In this paper, an experimental setup is used to investigate how the load-dependent properties such as stiffness and damping of the individual drives can be identified and modeled in order to use them for model-based controllers. The test bench is described in the following.

IV. EXPERIMENTAL SETUP

The test bench used for identifying the dynamic behavior of electrically preloaded rack-and-pinion drives is shown in Fig. 3. It consists of common industrial components, which are mentioned in the following. The rotary motion is generated by two permanent magnet synchronous motors from Siemens (1FT7086-5AH70-1CA0), which have a rated torque of 12.5 Nm. They are equipped with an AM24DQI motor encoder to obtain the motor position. The rotary motion is transmitted to the pinion (Wittenstein RMT400) by a two-stage planetary gearbox (Wittenstein RP040S) with a ratio of $i_g = 16$. The pinion, with a pinion pitch diameter $d_p = 0.08488$ m, transmits the force to the rack (Wittenstein ZST400) and the machine table performs a translational motion with a range of ~ 3 m. The total translational mass to be moved has a weight of $m = 403.8$ kg. The table position x_T is measured using a linear measurement system in the guide rails (Schneeberger AMSABS3). External forces simulating disturbances or milling processes can be applied by a linear direct drive (Siemens 1FN3300), which is mounted between

the guide rails under the table. The current control loop and the velocity control loop for the motors run on a control unit (Siemens CU320-2-DP). The position controller, the preload controller and the trajectory planning are implemented on a rapid control prototyping system.

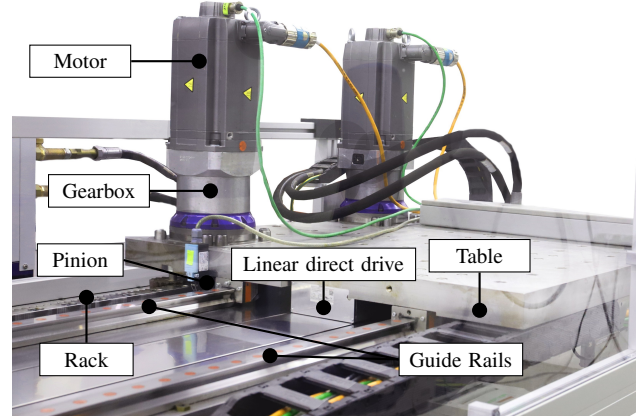


Fig. 3. The rack-and-pinion drive test bench used for identification and validation

V. MODELING OF THE LOAD-DEPENDENT PROPERTIES

The required measurements for the identification of the load-dependent properties are performed on the test bench. The influence of electrical preload on the properties of the RPD in terms of stiffness and damping as a function of load is investigated. To do this, the mechanical transfer function $G(s) = V_T(s)/V_1(s)$ is used. Frequencies in the range of $f \in [0.1, 400]$ Hz are excited with an amplitude v_a of 0.001 m/s for different preload torques. To eliminate the nonlinear effect of static friction, a small offset velocity v_{offset} of 0.005 m/s is added to the amplitude. The measurement is performed for a respective preload that varies in the range of 0% to 100% of the rated motor torque. Fig. 4 shows the mechanical frequency response of the system. It can be seen that the natural frequencies increase with increasing preload as well as the peak of the magnitude. Therefore, if a system is preloaded with higher torques, the natural frequency will increase and the position controller gain can theoretically be increased, thereby increasing the bandwidth of the system. A preload that adjusts according to the requirement is presented in [6] as an adaptive preload controller.

From the frequency response in Fig. 4, the transfer function and thus the natural frequency ω_0 , defined at the frequency where the phase is equal to -90° , can be determined. Due to the change in natural frequency, the stiffness of the system also changes. In the time domain it was seen that backlash occurs at small preloads and therefore cannot be represented in the FTF due to the nonlinearity of the backlash. Using ω_0 and neglecting the damping in the first step, the total stiffness of the system can be determined from $\omega_0 = \sqrt{k/m}$ by rearranging the equation to solve for the stiffness k . The mass m describes the total mass to be moved,

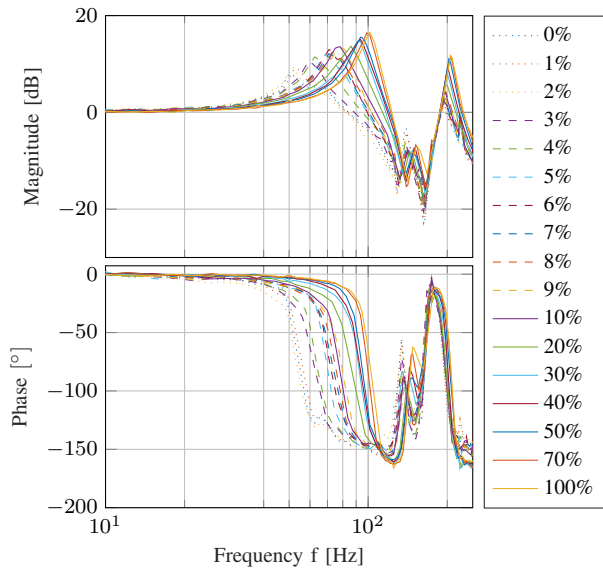


Fig. 4. Frequency response for different preload torques.

which is the mass of the table with motors, gearboxes, direct drive and the carriages, and can be determined in advance from data sheets. To determine the damping of the system from the mechanical frequency response, the damping ratio must be used. This characterizes the frequency response of the system. The damping ratio describes the actual damping d in a damped system to the critical damping d_c , where $D = d/d_c$. The stiffness is obtained from the natural frequency and the mass, and the damping d can be determined from the critical damping and the damping ratio:

$$k = \omega_0^2 \cdot m, \quad d = D \cdot d_c \quad (1a)$$

with

$$D = \frac{1}{2 \cdot |G(j\omega_0)|}, \quad d_c = 2 \cdot m \cdot \omega_0. \quad (1b)$$

Note that the above formulas hold, since the amplification factor for $G(s)$ is equal to 1. Due to the occurrence of backlash at small preloads (0% to 6%) at our test bench, these measurements are not considered in the further course. Thus, in Fig. 4, the stiffness and damping of the whole system can be obtained for a given preload. However, it is important to determine the stiffness and damping of the respective drive train. Varying the preload torque τ_p varies the respective motor torque, which is converted to the motor force using the conversion $2 \cdot i_g/d_p$ in the following. Fig. 1 shows the varying stiffness $k(F_i)$ and the varying damping $d(F_i)$ of the respective drive train as a function of the motor force. How the total stiffness and damping are assigned to the respective drive train is described in the following sections.

A. Stiffness

The stiffness for the overall system can be determined from the individual measurements for each preload. In the

preloaded system, where two identical motors act on each pinion, the amount of stiffness depends on the drive torque generated by the motor. Due to the preload, the motor forces are not equal during motion ($F_1 \neq F_2$) and therefore $k(F_1) \neq k(F_2)$. The total stiffness is a superposition of the respective drive train stiffness

$$k(F_1, F_2) = k(F_1) + k(F_2) \quad (2)$$

due to the arrangement of the springs in Fig. 1. Based on the frequency response, only the total stiffness $k(F_1, F_2)$ for a given preload can be determined using the equation for stiffness from (1a). The stiffness is calculated from the transfer function for each applied preload. As the preload increases, the natural frequencies and therefore the stiffness increase. It is now necessary to identify the total stiffness as a function of the two motor forces in order to model the stiffness as a function of load. For this purpose, it is assumed that the stiffness corresponds to a root function and that the function is determined for the identified total stiffness, taking into account the driving forces. The two-dimensional representation of the stiffness becomes a three-dimensional representation due to the two drive trains. The basic idea of the representation is illustrated in Fig. 5. Due to the preload and the resulting offset in the torque curves, motor 1 (M_1) and motor 2 (M_2) do not encounter backlash at the same time. If a drive does not apply any force to the rack (e.g. in backlash), the remaining stiffness is only provided by one drive and therefore the total stiffness decreases in this area. After the drive has gone through the backlash and the pinion is in contact with the rack again, the stiffness increases. This can be seen in Fig. 5 at the transition from e.g. ③ to ④ (red line for illustration) when motor 2 changes the sign of the driving force. The different motor configurations results in four quadrants where in ① both motors represent a positive force and in ③ both represent a negative force. In quadrants ② and ④ the drives are preloaded with different signs of the motor force.

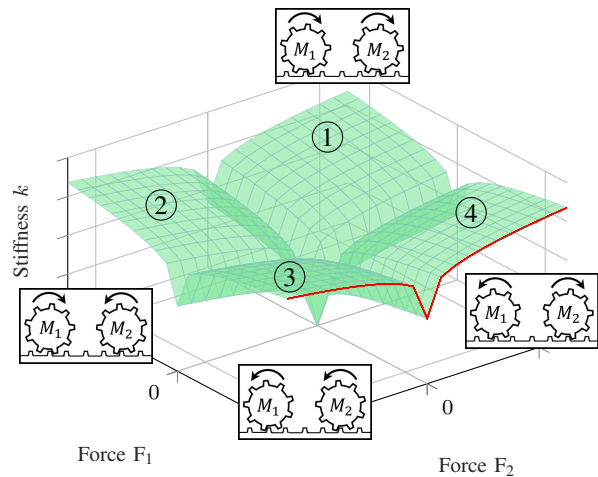


Fig. 5. Approach for calculating the stiffness depending on both forces.

To identify the surface, it is sufficient to consider only one quadrant in the following.

For the stiffness, the following empirically determined ansatz function is assumed

$$k(F_i) = k_1 \cdot k_2 \sqrt{|F_i|} \quad (3)$$

with two parameters k_1 and k_2 to be identified. To obtain the parameters, the particleswarm optimizer algorithm, described in [20], is used. This method is an iterative procedure to minimize the error between an assumed nonlinear function and the actual measured data. The sum of $k(F_1)$ and $k(F_2)$ provides the total stiffness

$$k(F_1, F_2) = k_1 \cdot k_2 \sqrt{|F_1|} + k_1 \cdot k_2 \sqrt{|F_2|} \quad (4)$$

depending on the respective motor force. Note that the parameters for both functions should be the same. The parameters are optimized by minimizing the normalized error between the stiffnesses k_{meas} determined from the measured frequency response and the stiffness calculated from the ansatz function $k(F_1, F_2)$ depending on the parameters,

$$[k_1^*, k_2^*] = \arg \min_{k_1, k_2} \sqrt{\frac{\mathbf{e}^\top \mathbf{e}}{\mathbf{k}_{\text{meas}}^\top \mathbf{k}_{\text{meas}}}} \quad (5a)$$

with

$$\mathbf{e} = \mathbf{k}_{\text{meas}} - \mathbf{k}(F_1, F_2). \quad (5b)$$

The parameters identified using particleswarm optimization converge to

$$k_1^* = 1.8709e7, k_2^* = 5.6406 \quad (6)$$

with a remaining error for the optimization function from (5a) of 4.01%. The ansatz function $k(F_1, F_2)$ from (4) represents the modeled stiffness from the frequency responses with the parameters mentioned.

Fig. 6 shows the model from (4) and the test bench measurements k_{meas} . Note that the measuring points are located close to the angle bisector due to the preload and the machine table movement. The total stiffness can therefore be divided into the two individual stiffnesses of the drive trains, represented by $k(F_1, 0)$ and $k(0, F_2)$, with one force being set to zero in each case. This provides the stiffnesses $k(F_1)$ and $k(F_2)$ needed for Fig. 1. Note that Fig. 6 only shows the quadrant for two positive motor forces. To represent the full range of stiffness, all four quadrants must then be considered as shown in Fig. 5.

B. Damping

To identify the load-dependent damping $d(F_1)$ and $d(F_2)$, the total system damping is determined from the transfer function and divided using the same method to identify the respective drive train damping from Fig. 1. The total damping of the system is again the sum of the two drive trains:

$$d(F_1, F_2) = d(F_1) + d(F_2) \quad (7)$$

To determine the damping d of the overall system, the equation for damping in (1) is used. The damping is also determined from the frequency response shown in Fig. 4. When calculating the damping, the preload changes the

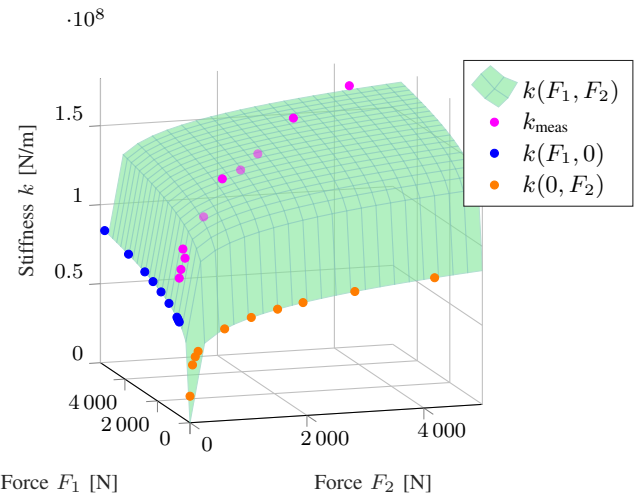


Fig. 6. Surface of the modeled stiffness depending on the measurements.

natural frequency and the amplitude gain at that frequency. The ansatz function assumed for damping, also determined empirically, is a hyperbolic function

$$d(F_i) = \frac{d_1}{d_2 + |F_i|} + d_3 \quad (8)$$

with three parameters (d_1 , d_2 and d_3) to be identified. Since the total damping from (7) depends on both driving forces, it can be determined as follows:

$$d(F_1, F_2) = \frac{d_1}{d_2 + |F_1|} + d_3 + \frac{d_1}{d_2 + |F_2|} + d_3 \quad (9)$$

The parameters d_1 , d_2 and d_3 are also obtained using particleswarm optimization. The ansatz function $d(F_1, F_2)$ is optimized to the measured points d_{meas} using the same optimization function from (5). The values for the parameters from the optimization are

$$d_1^* = 9.5376e5, d_2^* = 148.3813 \text{ and } d_3^* = 2.0734e4 \quad (10)$$

with a remaining error of 4.51%.

Fig. 7 shows the identified and modeled damping of the system in the quadrant of positive motor forces. The function from (9) with the parameters from (10) represents the total damping. The surface was approximated to the measurements from the frequency response d_{meas} and can now be divided to the respective drive train.

The load-dependent damping $d(F_i)$ from Fig. 1 can then also be distributed to the respective drive train and the respective damping of the drives on the table can be determined.

C. Validation

The stiffness and damping of the system have been identified and can now be modeled using the presented ansatz functions from (3) for stiffness and (8) for damping. Section V-A and Section V-B shows an analysis of how to divide the total stiffness and damping in a preloaded system. Figure 8 shows a comparison of the measured motor torques from the test bench and the simulated motor torques with

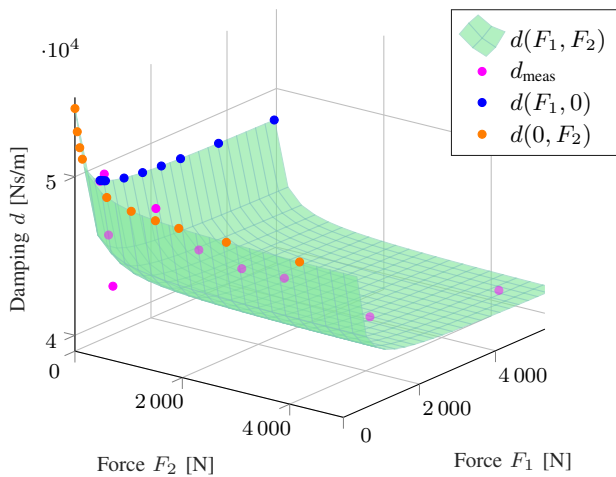


Fig. 7. Surface of the modeled damping depending on the measurements.

the modeled varying stiffness and damping. The simulation model is based on the three-mass oscillator from Fig. 1 with backlash. A time-optimal trajectory with a trapezoidal acceleration profile is used to validate the motor torques. The desired trajectory x_d is shown in the upper figure in Fig. 8 with $x_d \leq 1$ m, $|\dot{x}_d| \leq 0.5$ m/s, $|\ddot{x}_d| \leq 1$ m/s², $|\dddot{x}_d| \leq 20$ m/s³ and a preload of 10%. The quality of the fit is shown in Fig. 8 and a mean absolute error $J_\tau(e) = 1/M \sum_{i=1}^M |e_\tau|$ is used to evaluate. $J_\tau(e_1)$ is the error between the measured motor torque τ_1 and the simulated motor torque $\tau_{1,\text{sim}}$ and is $J_{\tau_1}(e_{\tau_1}) = 0.4042$ Nm. For motor 2 the mean absolute error between τ_2 and $\tau_{2,\text{sim}}$ is $J_{\tau_2}(e_{\tau_2}) = 0.3271$ Nm.

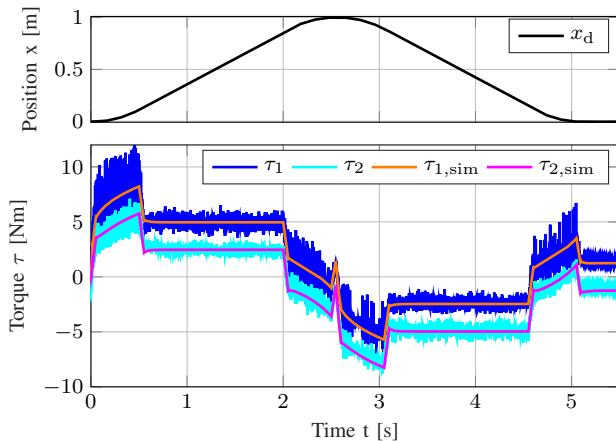


Fig. 8. Comparison of measured and simulated motor torques with varying stiffness and damping.

A novel load-dependent stiffness and damping model for electrically preloaded systems was derived and experimentally validated.

VI. CONCLUSION

This paper presents a method for determining the load-dependent system properties of stiffness and damping for each drive train in a preloaded system. Due to the preload,

only the overall stiffness and damping of the physical machine can be identified. A three-mass oscillator, which represents the preloaded system, illustrates the coupling between stiffnesses and between dampings. The paper is motivated by the nontrivial partitioning of the identified total stiffness and damping from the frequency response and proposes an approach to model these properties with ansatz functions for the particular drive train. The parameters of the functions are determined with a particleswarm optimizer to obtain precise modeling of those properties. Finally, the load-dependent modeling of the stiffness and damping was validated in the time domain and shows small deviations in the resulting motor torques from the measured data on the test bench.

For electrically preloaded systems, the presented method can now be used to determine the appropriate part of the drive train and allow more accurate modeling. The focus of this paper is on the method of distributing stiffness and damping to the drive train. The modeled and identified properties can be used for the representation of the test bench in a simulation model, for reconstructions and observer concepts, since these system properties are also required there. For example, to increase the accuracy of indirect controlled and preloaded RPDs, the table position can be reconstructed based on the respective motor encoder, including stiffness, see [21]. The reconstruction can now be extended to include the load-dependent stiffness in the system with the approach in this paper. To further increase the accuracy of the system, only the reconstructed signal from the motor, which is not affected by the backlash, can be fed back into the position control loop using smooth switching with two sigmoid weighting functions. This will be demonstrated in future work.

In addition, the approach of this paper can also be considered to develop a new control concept for preloaded systems. In particular, for an adaptive preload controller of the two motors, the representation from Fig. 5 can be used to control the preloaded systems with a certain stiffness along the surface. In this way, the preload can be adjusted to maintain a certain level of stiffness under different operating conditions.

REFERENCES

- [1] T. Engelberth, *Adaptive Verspannung von Zahnstange-Ritzel-Antrieben*. Stuttgart: Fraunhofer Verlag, 2020.
- [2] S. Frey, A. Dadalau, and A. Verl, "Expedient modeling of ball screw feed drives," *Production Engineering*, vol. 6, no. 2, pp. 205–211, 2012.
- [3] Y. Altintas, A. Verl, C. Brecher, L. Uriarte, and G. Pritschow, "Machine tool feed drives," *CIRP annals*, vol. 60, no. 2, pp. 779–796, 2011.
- [4] L. Uriarte, M. Zatarain, D. Axinte, J. Yagüe-Fabra, S. Ihlenfeldt, J. Eguia, and A. Olarra, "Machine tools for large parts," *CIRP annals*, vol. 62, no. 2, pp. 731–750, 2013.
- [5] T. Engelberth, S. Apprich, J. Friedrich, D. Coupek, and A. Lechler, "Properties of electrically preloaded rack-and-pinion drives," *Production Engineering*, vol. 9, no. 2, pp. 269–276, 2015.
- [6] A. Verl and T. Engelberth, "Adaptive preloading for rack-and-pinion drive systems," *CIRP Annals*, vol. 67, no. 1, pp. 369–372, 2018.
- [7] N. L. de Lacalle and A. L. Mentxaka, *Machine tools for high performance machining*. Springer Science & Business Media, 2008.
- [8] O. Zirn, "Machine tool analysis: modelling, simulation and control of machine tool manipulators," Habilitation Thesis, ETH Zurich, 2008.

- [9] C. Brecher and M. Weck, *Machine Tools Production Systems 3: Mechatronic Systems, Control and Automation*. Wiesbaden: Springer Fachmedien Wiesbaden GmbH, 2022.
- [10] H. Dai, X. Long, F. Chen, and C. Xun, "An improved analytical model for gear mesh stiffness calculation," *Mechanism and Machine Theory*, vol. 159, p. 104262, 2021.
- [11] L. Steinle, A. Lechler, M. Neubauer, and A. Verl, "Experimental investigation into the implications of transmission errors for rack-and-pinion drives," *Production Engineering*, pp. 1–11, 2021.
- [12] V. Vullo, *Gears: Volume 1: Geometric and Kinematic Design*, 1st ed., ser. Springer Series in Solid and Structural Mechanics. Cham: Springer International Publishing and Imprint Springer, 2020, vol. 10.
- [13] N. L. Pedersen and M. F. Jørgensen, "On gear tooth stiffness evaluation," *Computers & Structures*, vol. 135, pp. 109–117, 2014.
- [14] R. Neugebauer, *Werkzeugmaschinen: Aufbau, Funktion und Anwendung von spanenden und abtragenden Werkzeugmaschinen*. Springer-Verlag, 2013.
- [15] L. Chang, G. Liu, and L. Wu, "A robust model for determining the mesh stiffness of cylindrical gears," *Mechanism and Machine Theory*, vol. 87, pp. 93–114, 2015.
- [16] T. Kiekbusch, D. Sappok, B. Sauer, and I. Howard, "Calculation of the combined torsional mesh stiffness of spur gears with two-and three-dimensional parametrical fe models," *Strojniški vestnik-Journal of Mechanical Engineering*, vol. 57, no. 11, pp. 810–818, 2011.
- [17] M. B. Sánchez, M. Pleguezuelos, and J. I. Pedrero, "Approximate equations for the meshing stiffness and the load sharing ratio of spur gears including hertzian effects," *Mechanism and Machine Theory*, vol. 109, pp. 231–249, 2017.
- [18] M. Ankouni, "Modeling of damping in elasto-hydrodynamic lubricated contacts: Application to gear dynamics," Ph.D. dissertation, Université de Lyon, 2016.
- [19] L. D. Mitchell, "Improved methods for the fast fourier transform (fft) calculation of the frequency response function," *Journal of Mechanical Design*, vol. 104, no. 2, pp. 277–279, 1982.
- [20] R. Eberhart and J. Kennedy, "A new optimizer using particle swarm theory," in *MHS'95. Proceedings of the Sixth International Symposium on Micro Machine and Human Science*, 1995, pp. 39–43.
- [21] T. Engelberth, M. Neubauer, and A. Verl, "Master-switch für verspannte zahnstange-ritzel-antriebe: Genauigkeitssteigerung indirekt lagegeregelter systeme," *atp magazin*, vol. 61, no. 3, pp. 54–63, 2019.